Title

NONEQUILIBRIUM MICROSTRUCTURES ; LECTURE 6: 2nd CONFERENCE ON MATERIALS SCIENCE, TREMEZZO, ITALY, SEPTEMBER 14-25, 1970

Author

Thomas, G.

Publication Date

1970-11-01

Lectures for 2nd Conference
on Materials Science, Tremezzo,
Italy, September 14-25, 1970

UCRL-19698
c. 2

LECTURE 6: NONEQUILIBRIUM MICROSTRUCTURES

G. Thomas

November 1970

AEC Contract No. W-7405-eng-48

LAWRENCE RADIATION LABORATORY
UNIVERSITY of CALIFORNIA BERKELEY

UCRL-19698
c. 2

DISCLAIMER

LECTURE 6: NONEQUILIBRIUM MICROSTRUCTURES

G. Thomas

Inorganic Materials Research Division, Lawrence Radiation Laboratory
Department of Materials Science and Engineering, College of Engineering
University of California, Berkeley, California

Introduction

The properties of a material depend on all the elements of its structure: from the atom and its components, atom aggregates and lattice defects which comprise the microstructure[1], the macrostructure and finally the structural member or device itself[2]. Physical metallurgy or materials science is concerned mainly with the microstructures and their effects on properties. In practical materials the microstructures are almost always in non-equilibrium. Ideally when these relations are completely understood they can be controlled and consequently these aspects will lead to important new contributions in alloy design[3-5]. The range of microstructures of interest here varies in scale from angstroms to millimeters and comprises dislocations to grains. If metals were free from defects they would behave ideally and have very high strengths. However, because it is not possible to manufacture large pieces of metals without grain boundaries or other defects at which dislocations can be generated and move and multiply at rather low stresses, high strengths can only be achieved practically by designing alloys in which microstructures can be produced which limit dislocation motion. Whilst this is not difficult to do it is at the same time very difficult to achieve all the other desirable engineering properties, for example ductility, toughness, fatigue, creep and corrosion resistance amongst others. This is the main challenge to physical metallurgists today.

Since it is impossible to cover the whole field of physical metallurgy here*, we propose to indicate some general features that are important in areas such as mechanical properties and alloy design

---

* See the main references cited also for lectures 3,4,5.

and which attempt to link the material given in the earlier lectures. The illustrations used are derived from existing research programs at Berkeley. The references are typical but are not comprehensive.

Strengthening of Metals.

The methods of strengthening metals all relate to providing obstacles to dislocations.[3-8] The yield strength $\tau_y \simeq Gb/L$ where G is the shear modulus, b is the Burgers vector of dislocations and L is the separation of obstacles. If τ_y ideal = G/7.5 the limit on L is about 15 atom diameters. Examples of obstacles and methods which can be efficient in strengthening include the following:

1. Dislocation-Dislocation Strengthening: Dislocations can be introduced by plastic deformation to cause work hardening. However, there is a limit to the amount of plastic deformation that metals can wtihstand without fracturing. One of the most successful strengthening cold working processes is wire drawing in which high densities of dislocations are arranged in small cells elongated along the drawing direction. It is very difficult, however, to obtain uniform distributions of dislocations since in uniaxial deformation, bands or cell structures develop (fig. 1). However, high strain rates such as explosive deformation (fig. 2) and shear transformations such as martensitic or bainitic reactions can give rise to high densities of uniformly distributed dislocations (figs. 3,4).

Dislocated martensites are generally tougher than twinned martensites even at the same yield strengths (fig. 5) so that control of composition and processing is important, since the transformation substructure is composition dependent as indicated in Table 1.[9] Generally the carbon content in austenite must be less than about

0.3% if twinning is to be avoided and the richer the solute content the greater is the probability of twinned martensite. The most likely reason that twinned martensites have poor toughness characteristics is that they themselves deform plastically by twinning rather than slip and twinning is not useful in preventing crack growth (see fig. 3 of my previous chapter). Thus, if the structure or microstructure restricts plastic deformation by slip the toughness deteriorates.

TABLE I

STRUCTURE OF BODY-CENTERED FERROUS MARTENSITES FORMED ON COOLING THROUGH Ms-M_f*

Alloy System	Ms	Substructure/Composition**
Fe-C	>350°C	C < 0.3 mainly dislocated laths
	<250°C	C > 0.6 mainly twinned plates
Fe-Ni	>-50°C	Ni < 25 dislocated laths
	-30°-150°C and below	Ni ≥ 30 mid-rib twinned only
		Extent of twinning increases with % Ni, and lower M_s
Fe-Ni-C	as above	Increase in carbon for same nickel content & vice-versa enhances twinning
Fe/25Ni/0.3C/4.5Mo	<-77°C	All mainly twinned. However ausforming causes precipitation of carbides, so that the resulting martensite is less twinned.
+4.7 Cr	-16°C	
+1.85V	-3°C	
Fe-Ni-Co-C (1/2Mo/1/2Cr)	~260°C	C < 0.3 dislocated laths
	150-260°C	C > 0.4 twinned
		cobalt does not decrease twinning.

Fe/Cr/C	350-400°C	Partially twinned Cobalt raises Ms - does not decrease % twinning
Fe-5Cr		dislocated laths
Fe-8Cr-1C	-30°C	twin density decreases with increasing plate size
Fe/5Ni/0.25C	315°C	mainly dislocated
Fe/3Mn/0.25C	315°C	mainly dislocated
Fe/5Ni/7Mn/0.25C	65°C	mainly twinned
Fe/7Mn/0.25C	190°C	mainly twinned for a given carbon level, manganese promotes twinning.
Fe/Ni/Ti		dislocations and twins depend on Ni/Ti & heat treatment
Fe/Cr/Ni	metastable austenites	low stacking fault energy dislocated α from ε

* All data here refer to nominal cooling rates. The Ms temperature and structure can be varied by varying quench rate.

** Compositons refer to weight %.

A fine distribution of dislocation cells is analogous to fine scale grain size strengthening. The barrier distance L is about half the cell (or grain) size. The cell walls or grain boundaries can trap as well as emit dislocations. A practical limit on L by this class of strengthening is 0.5 to 0.1μ, corresponding to yield strengths of ~ G/100.

2. Particle strengthening:

In this scheme large numbers of second phase particles are required.[3,4,6,7] They can be produced by special techniques of dispersing hard intermetallics such as oxide particles (e.g. SAP Al, TD Ni) by heat treatment such as in age hardening aluminum alloys and structural steels, or by more complex thermal-mechanical treatments used for alloy steels. The properties of the matrix are determined by the dislocation-particle interactions and are influenced by the relative strengths of matrix and particle and the nature of the interface (coherent or not) (Fig. 6). The properties of the alloy in total however also depend on the grain boundary structure and properties. The strength of the grain boundaries is not usually equivalent to that of the matrix and if these differences are large, intergranular failure becomes common. One of the factors leading to this failure is the development of non-uniform microstructures at and near the boundaries. A famous brittle example is in the Al/Zn/Mg type of high strength alloy in which hard $MgZn_2$ particles form along the boundary, but adjacent to the boundary a precipitate free zone exists in which nucleation of precipitates is difficult probably due to the loss of vacancies to the boundary itself.[10] This kind of heterogeneous nucleation is typical of many alloys but is not found in

homogeneous precipitation systems such as spinodals for which there is no nucleation barrier. Figure 7 is a dramatic example of the morphological differences between these systems. This is not to say that the spinodal microstructure necessarily means the avoidance of intergranular failure. Segregation can be detected by microprobe techniques even though the microstructure appears to be uniform, and in the previous chapter examples were shown of the fractography (fig. 8) and segregation (fig. 22) in the Cu/Ni/Fe spinodal. Another difficulty with these grain boundary phenomena is corrosion and stress corrosion susceptibility which is closely related to restricted plastic flow in the grain boundary region.

Precipitation produced by solution heat treatment and aging can also lead to heterogeneous microstructures within the matrix. The quenching treatment retains large numbers of vacancies which can condense to dislocation loops, form helices, etc. upon which preferential precipitation is favored (nucleation barrier reduced). Figure 17 of the last chapter is an example of this effect in Al-Cu alloys. The aging is done to produce mainly the θ'' phase but large θ' particles have nucleated and grown from dislocations. These regions seem to cause fatigue failure due to preferential slip there.[10] The yield strength variation with aging in the Al/Cu system is indicated in fig. 8. The ductility varies inversely. This behavior is typical of aging systems including ferrous alloys.[7,12]

As indicated earlier the morphology of precipitation strengthened systems depends on the nucleation criteria and on the strain energy factor.[12]

The latter controls the particle shape. Spheres, plates and rods are all well known features in Al alloys. The larger the strain energy, the less tendency there is for coherency, and incoherent interfaces tend to promote internal cracks by fracture along the interface of the particle and its matrix. Thus the nature of the interface is very important in affecting the slip characteristics.

Table 2 summarizes the features discussed in the above. Figure 9 summarizes the obstacle strengthening principle in relation to the properties that are currently attainable. The gap is still too large between theoretical possibilites and actual achievements.

The character of the microstructure is also important in affecting the properties of steels which are heat-treated by conventional quench-tempering methods or isothermally to lower bainite. The fine structure of martensite is related to the transformation shears which can be slip or twins or both, Table 1. Recent observations indicate that dislocated martensites have superior toughness compared to twinned martensites of the same yield strengths (fig. 5). As a result of these observations (e.g. ref. 14) it seems that isothermal annealing to form lower bainite may be superior heat treatment to quench/tempering since lower bainites are not twinned and are tougher than the twinned alloy of the same composition. However, tempering can produce embrittlement by precipitation of carbides along the dislocations, e.g. at lath boundaries. Impurity segregation is also important.

Special, more complicated processing involving thermal/mechanical treatments have been successful in obtaining strong and ductile steels, e.g. ausforming[3] and "tripping"[15] which differ only in the manner

Table 2

Dispersions	Characteristics	Methods of Producing
Ductile	Low to moderate strength, good ductility	Age-hardening (Al alloys alloy steels)
Spinodals	High strength possible but poor ductility common	Heat treatment as for age-hardening
Refractory	Very high strengths possible with poor or moderate ductility	Compacting, powder metallurgy as in Ni and W base alloys. Special processes, e.g. Dupont TD Ni. Internal oxidation of an alloy so as to cause one component to precipitate as an oxide. Fiber techniques. Eutectic alloys. Combination of thermal-mechanical treatments, e.g. strain aging, ausforming.

in which the transformation is effected (fig. 10). The strengthening response in ausformed steels is largely a result of precipitation-dislocation strengthening, i.e. deformation of metastable austenite results in precipitation of carbides and the latter cause dispersion hardening and dislocation multiplication as dislocations are generated during the austenite-martensite shear transformation on cooling below Ms.[3] In the "TRIP" process the austenite is strengthened by deformation and martensite is strain induced by deformation above Ms but below Md.[15] The resulting martensite shows extremely fine laths as compared to conventional or ausformed martensites (fig. 11) so there is considerable substructural refinement and strengthening. The important benefit, however, is that high toughness is obtained because the transformation to martensite is effective in preventing necking. More details of these new and exciting techniques are given in Professor Parker's lectures.

Dislocation Configurations

The dislocation configuration is determined by the "state" of the matrix as well as by the general microstructure (particles, etc.). Thus the lower the stacking fault energy SFE or the higher the degree of order, the less easy it is for dislocations to cross slip and so they tend to be confined to slip planes. An important consequence of this restriction on cross-slip is that susceptibility to transgranular stress corrosion increases.[3,16] A well known system is that of austenitic stainless steels. The stress corrosion susceptibility is known to decrease with increasing nickel and nickel decreases the SFE.[17,18] It is thought that one of the factors related to the stress corrosion

susceptibility is that intense slip bands lead to large surface steps which can disrupt surface protective films; if cross slip is easy the dislocations can slip out of the main slip bands and form small surface steps which may not disrupt the surface film. Thus slip structures that are associated wtih complex dislocation tangles are preferable to those that are associated with planar groups. As shown in figs. 6,7 of my first lecture, the changes in slip structure and stacking fault energy correlate very well with the known transgranular corrosion susceptibility of α-brasses. High voltage electron microscopy is a useful tool for investigating these phenomena.[19]

Two other examples are given now to indicate where electron microscopy methods have provided important new information which would be difficult or impossible to obtain indirectly.

Interstitial Impurities in Refractory Metals.

It has been known for a long time that as the interstitial solute content increases in the refractory metals, the system becomes embrittled particularly at low temperatures, and so the ductile-brittle transition temperature is raised as the solute content is increased. This is illustrated for pure tantalum and various Ta-C alloys in fig. 12.

In this system and in other metals of groups V where the solubility of interstitials is greater than 1 at.% the phenomenon of interstitial ordering has been discovered[20] and recent work by electron microscopy and diffraction on Ta-C indicates that the embrittlement is associated with the formation of compounds such as $Ta_{64}C$. This compound developes by an ordering process similar to that of short range order in substitional

alloys involving microdomains on {110} planes as shown in fig. 13.

Diffusion Induced Defects.

A detailed investigation of the defects produced in silicon as a result of doping treatments with phosphorus and boron showed that due to the change in lattice parameter accompanying diffusion of the solute, a solute contraction stress is set up which results in the formation of dislocation networks (see fig. 14).[21] In the case of a npn transistor formed by double diffusion of P and B, precipitates have been found near the emitter surface (in the n-type layer). These precipitates form as plates on {111}, and it appears that these are produced concomittantly with the dislocations in such a way as to minimize the solute contraction stress, i.e., they are produced during the diffusion and not after subsequent cooling down. This result is deduced from the micrographs of Fig. 15. In 15(a) only one set of precipitates has formed on $(11\bar{1})$ and only one set of dislocations is seen, these lying normal to the precipitates along $[11\bar{1}]$. The Burgers vector of these dislocations is $a/2\ [1\bar{1}0]$ and they are pure edge. Contrast experiments on the precipitates showed that they are extrinsic in sense and with displacements in <111> normal to the habit plane. Thus, in [112] one set of edge dislocaitons and a set of precipitates normal to the dislocations can minimize the solute contraction stress. Thus precipitates always form in {111} planes most nearly normal to the diffusion front. In this respect precipitates and dislocations are equivalent and equivalent patterns of dislocations and precipitates are formed for other crystal orientations, e.g. fig. 15b. The extrinsic character of the precipitates has been confirmed from diffraction

patterns, e.g. Fig. 16. The precipitate patterns index as base centered orthorhombic (e.g. Fig. 1c) with a = 3.8Å, b = 6.6Å, c = 6.75Å. The axis is parallel to the [111] Si, hence one unit cell of the precipitate in the matrix can be regarded as an extrinsic Frank defect of displacement vector slightly larger (~7%) than 1/3[111]. Thus the "strength" of the precipitate is less than that of a dislocation (b = a/2<110>) and so for equivalent stress relief, the precipitate spacing is less than that of the dislocation spacing (fig. 15a).

The importance of structure-property relations with regard to electrical/magnetic behavior of solids is only just being exploited. Meanwhile continued and rigorous progress is being made in the understanding of the mechanical behavior of materials in terms of microstructure and atomistic processes.

ACKNOWLEDGEMENTS

This work was done under the auspices of the U.S. Atomic Energy Commission through the Lawrence Radiation Laboratory at Berkeley.

1. W. Hume-Rothery, R. E. Smallman and C. W. Haworth, Structure of Metals and Alloys, Metals and Metallurgy Trust Mon #1, 1969.
2. E. R. Parker, Problem Areas in Engineering Design Fracture Univ. of Melbourne, Tewkesbury lecture, 1969, p. 9.
3. High Strength Materials, Ed. V. F. Zackay, Wiley, N.Y. (1965).
4. G. Thomas, E. R. Parker and V. F. Zackay, Strengthening Mechanisms in Metals and Ceramics, Syracuse Univ. Press, 1966, p. 3.
5. Journal Iron and Steel Inst. 207, (6) 1969, Centennial Issue.
6. Strength of Metals and Alloys, Japan Inst. of Metals, Special Supplement to vol. 9, 1968.
7. A. Kelly and R. B. Nicholson, Prog. Mat. Sci. 10, 151 (1963).
8. A. H. Cottrell, Mechanical Properties of Matter, Wiley, 1968.
9. Symposium on Martensite, AIME 1970, Gordon and Breach (in press).
10. G. Thomas and J. Nutting, J. Inst. Met. 88, 81 (1960).
11. C. Laird and G. Thomas, Int. J. Fracture Mechs. 3 (2) 81 (1967).
12. G. Thomas and J. Washburn, Eds., Electron Microscopy and Strength of Crystals, J. Wiley, 1963.
13. J. W. Christian, Theory of Phase Transformations, Oxford, 1967.
14. S. K. Das and G. Thomas, Trans. ASM 62, 659 (1969).
15. V. F. Zackay, E. R. Parker, D. Fahr and R. Busch, ASM Trans. 60, 252, 1967.
16. Fundamental Aspects of Stress Corrosion Cracking, 1969.
17. P. R. Swann, Corrosion 19, 102 (1962).
18. D. L. Douglass, W. R. Roser and G. Thomas, Ibid., 20, 15 (1964).
19. P. R. Swann and J. R. Duff, Met. Trans. 1(1) 69 (1970).
20. R. E. Villagrana and G. Thomas, Phys. Stat. Solidi 9, 499 (1965).
21. E. Levine, G. Thomas, and J. Washburn, J. Appl. Phys. 38, 81,87 (1967).

FIGURE CAPTIONS

Fig. 1. Dislocation cell structure typical of tensile deformed metals. Nickel deformed 20% elongation at 295°K. Courtesy Acta Met.

Fig. 2. Dislocation structure in explosively deformed nickel. The shock pressure left to right was 70kb, 130kb, 250kb. Shock direction given by arrow c. Courtesy Acta Met.

Fig. 3. Dislocated martensite in low alloy manganese bearing steel. Courtesy D. Huang

Fig. 4. Dislocations and iron carbide particles in lower bainite of low alloy steel. Courtesy D. Huang

Fig. 5. Showing the dependence of toughness on microstructure for steels of similar yield strengths; twinned steels have poorer toughness Fe/Ni/Co/C alloys. ref. 14. Courtesy Transactions ASM.

Fig. 6. Idealized stress strain curves indicating behavior of yield strength and work hardening rates on microstructure. #3 pure metal.

Fig. 7. Grain boundary morphologies in age-hardening alloys a) Al-Mg-2n b) spinodal Cu/Ni/Fe.

Fig. 8. Typical age hardening response of Al-Cu alloys.

Fig. 9. Theoretical strength of metals determined by undeformable barrier strengthening only.

Fig. 10. Schematic showing techniques for a) the trip process, b) ausforming process. Notice in (c) the greater ductility of trip alloys at equivalent strength levels.

Fig. 11. Microstructures of the same steel a) as quenched, lath martensite, b) deformed austenite, c) trip martensite. Notice the marked refining of martensite after trip processing. (after M. Raghavan)

Fig. 12. Tensile elongation vs. temperature for Ta and Ta-C alloys. Courtesy P. Rao.

Fig. 13. The ordered domain structure corresponding to the formation of the interstitially ordered phase $Ta_{64}C$ in Ta-1.5%C. Courtesy P. Rao.

Fig. 14. Diffusion induced dislocations in 110 slice of silicon. This is a stereo pair (align dots for viewing by stereopticon) ref. 21. Courtesy J. Appl. Phys.

Fig. 15. a) Diffusion induced precipitates and dislocations near emitter surface of [112] silicon. b) As a), [111] orientation. ref. 21. Courtesy J. Appl. Phys.

Fig. 16. Diffraction pattern from edge-on precipitates shown in 15(a). In a) orientation is [112], in b, c it is [011].

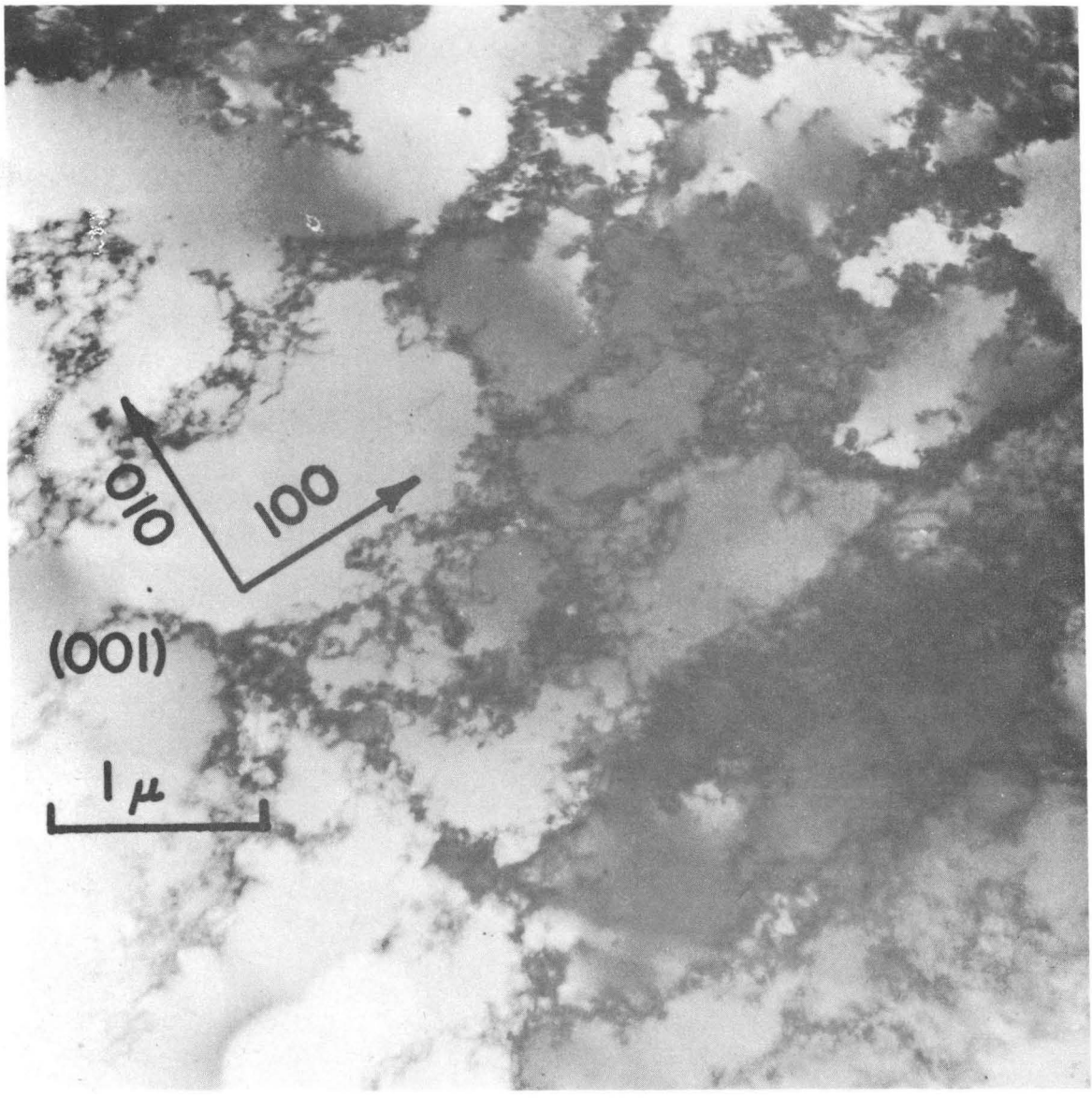

IM664

Fig. 1.

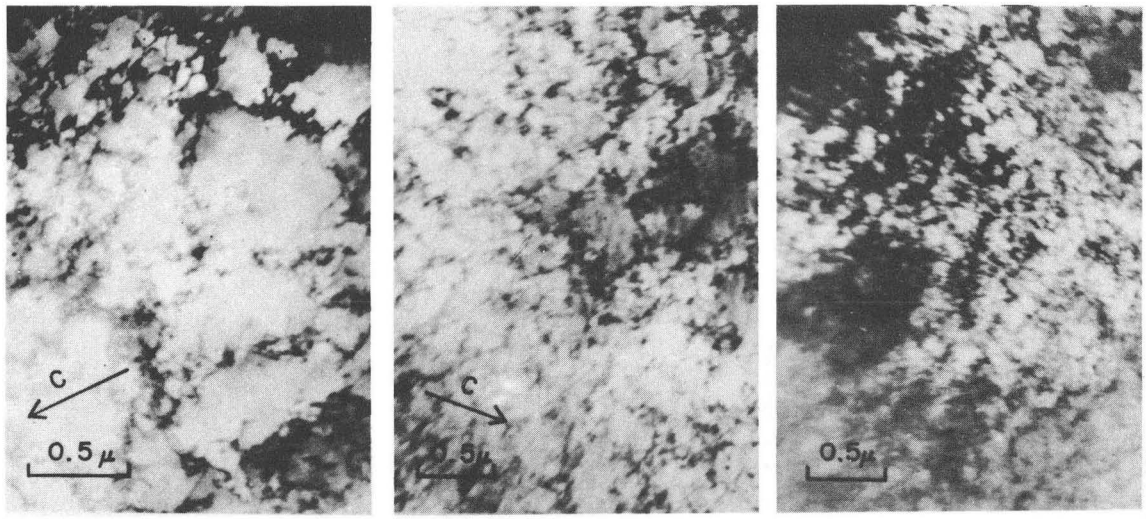

IM657

Fig. 2.

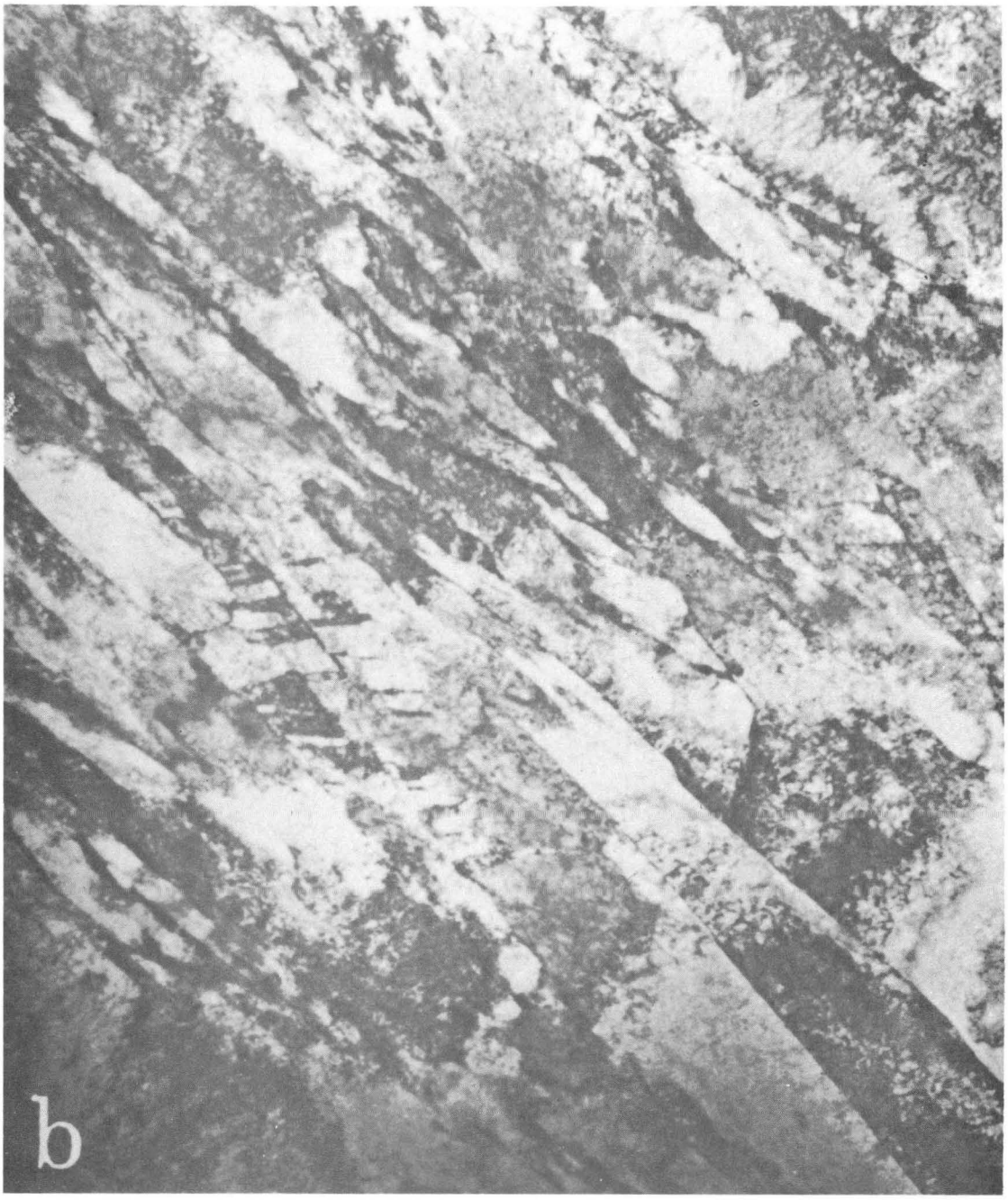

XBB698-5583-A

Fig. 3.

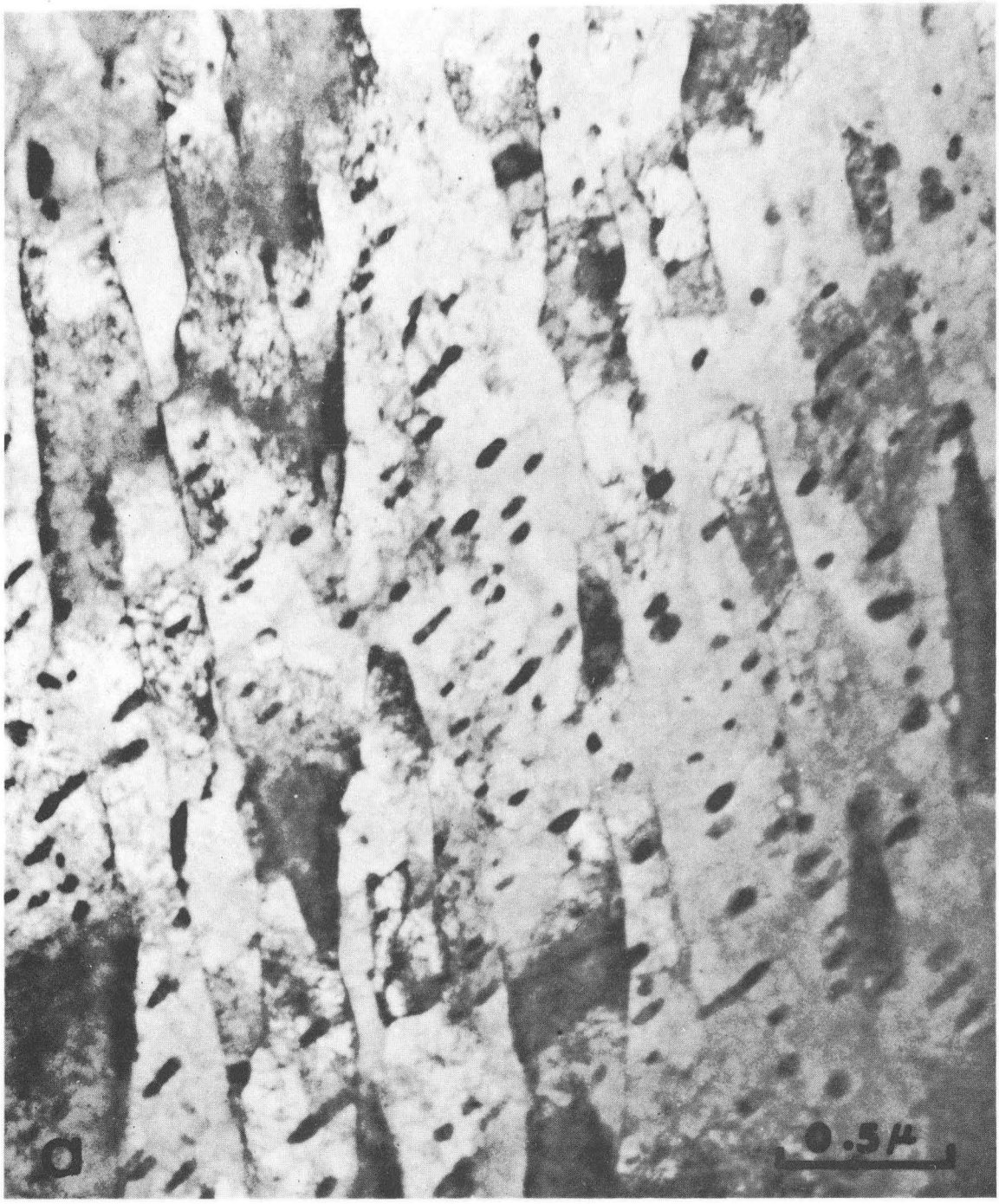

XBB698-5561-A

Fig. 4.

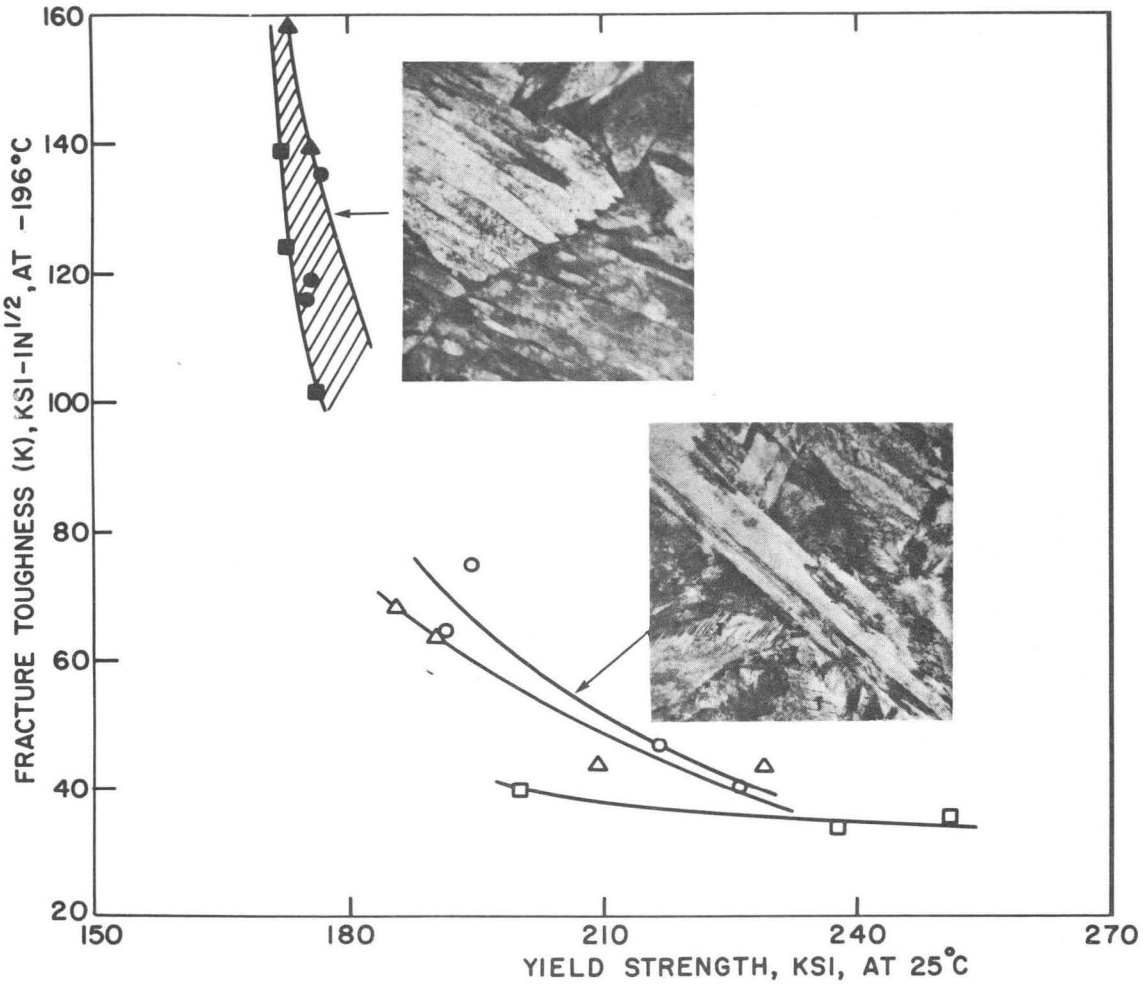

XBB701-475

Fig. 5.

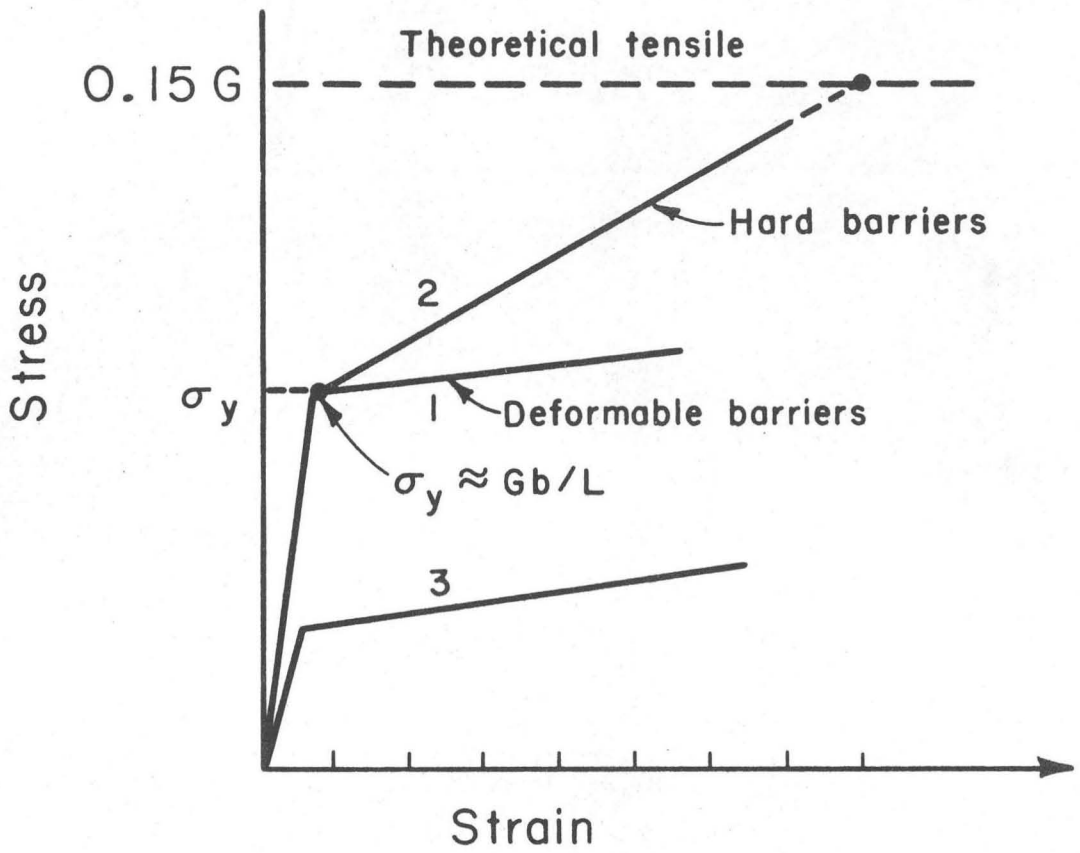

MUB-6751

Fig. 6.

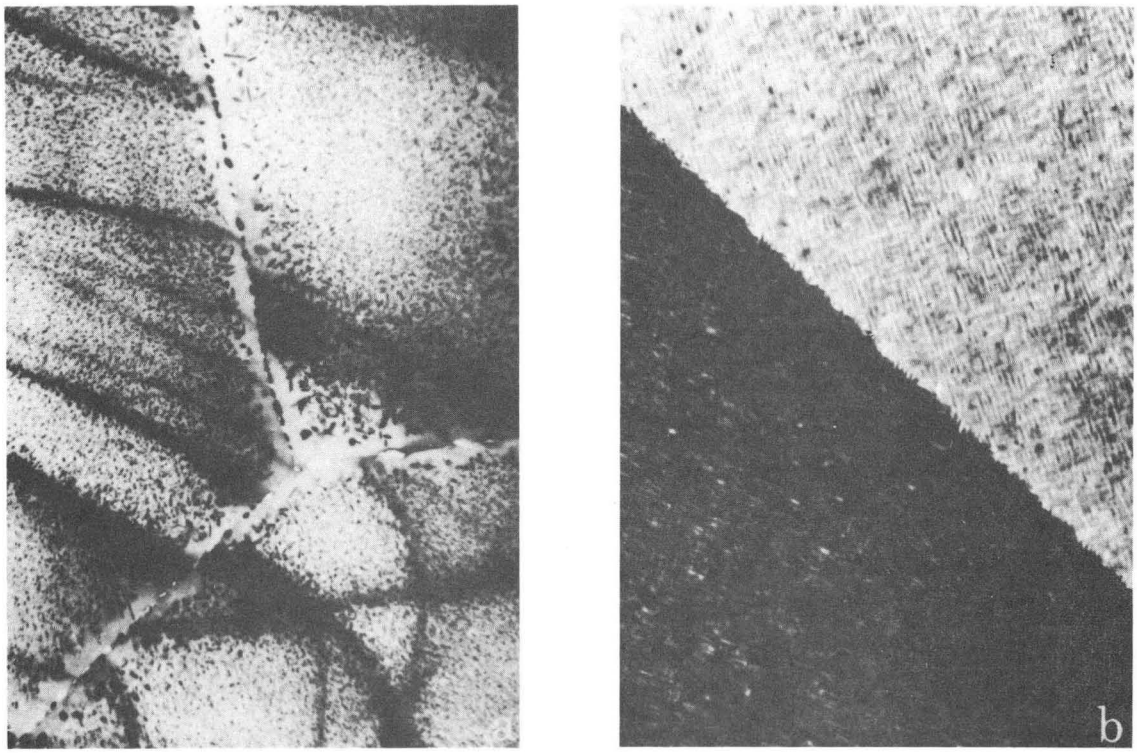

XBB695-3420-A

Fig. 7.

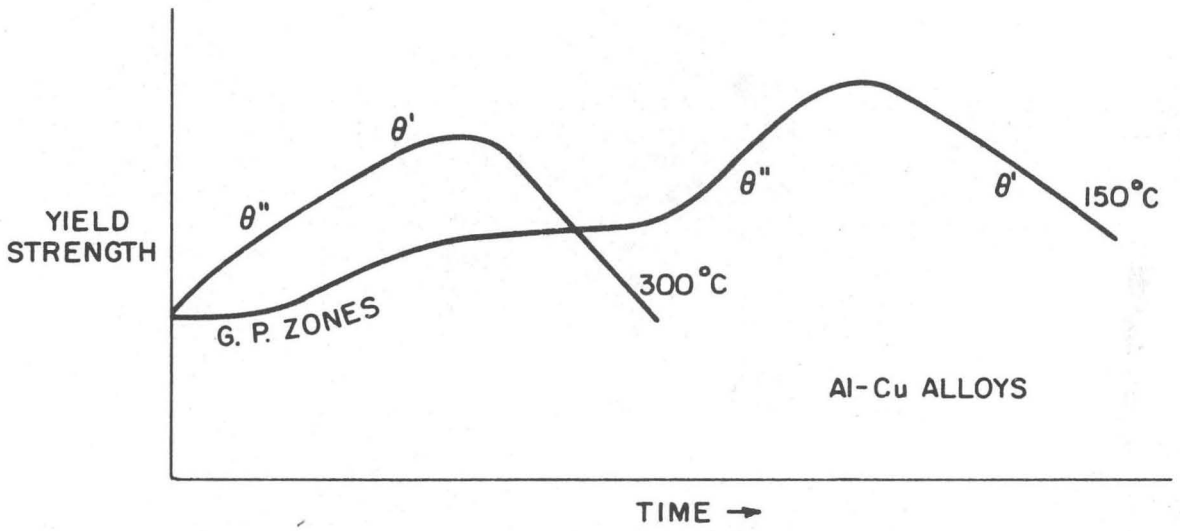

XBL 708-1891

Fig. 8.

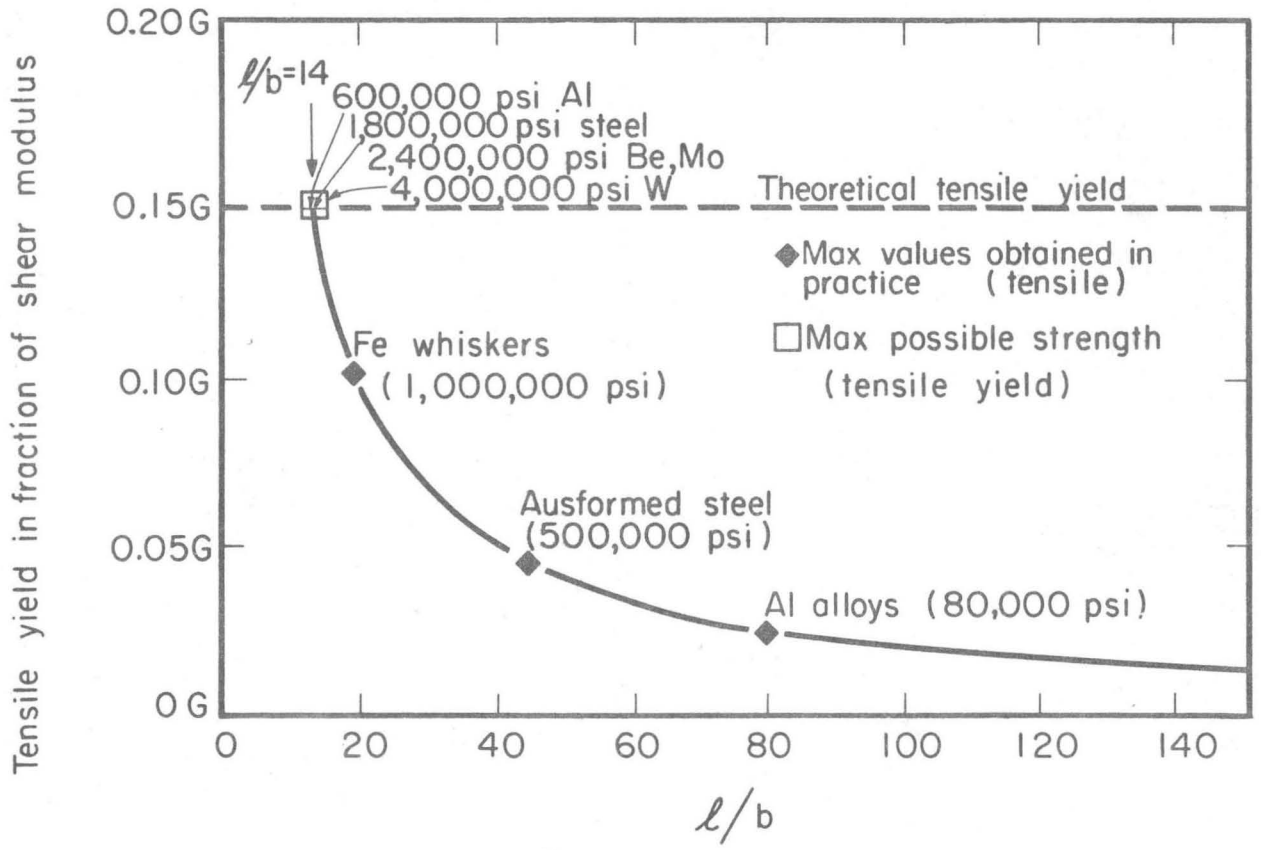
Tensile yield in fraction of shear modulus
0.20G
0.15G
0.10G
0.05G
0 G
0
20
40
60
80
100
120
140
ℓ/b
ℓ/b=14
600,000 psi Al
1,800,000 psi steel
2,400,000 psi Be,Mo
4,000,000 psi W
Theoretical tensile yield
◆Max values obtained in practice (tensile)
□Max possible strength (tensile yield)
Fe whiskers (1,000,000 psi)
Ausformed steel (500,000 psi)
Al alloys (80,000 psi)
MUB-6755

Fig. 9.

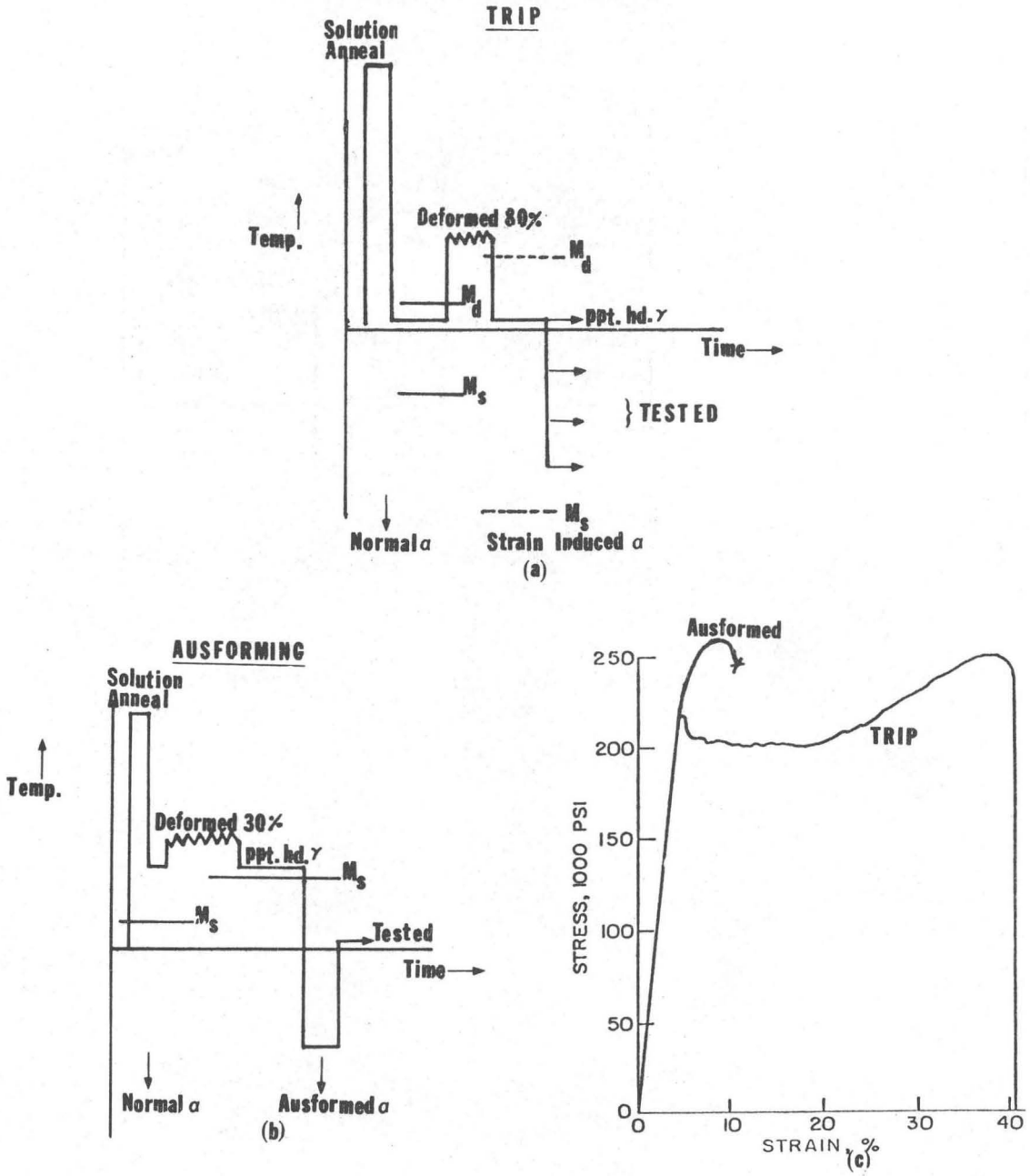

XBL 708-1748

Fig. 10.

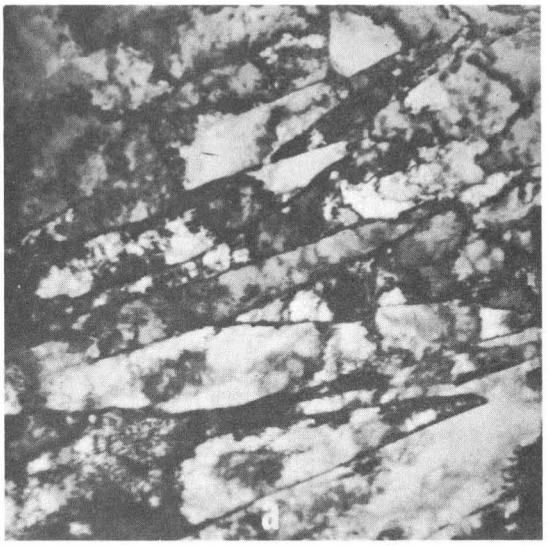

α [M_s -90°C, M_d 55°C]

μ

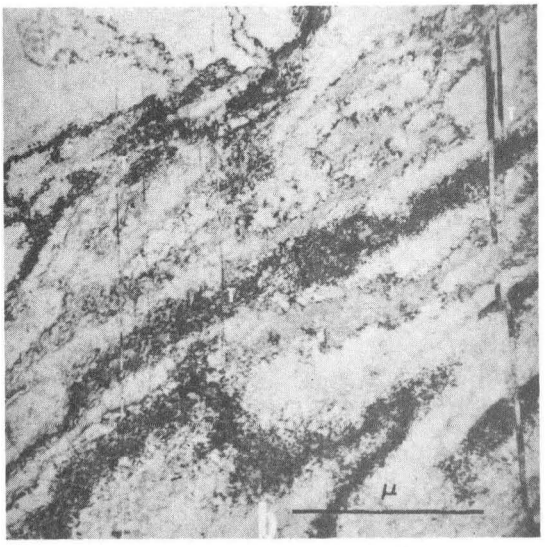

γ - rolled 20% at 250°C

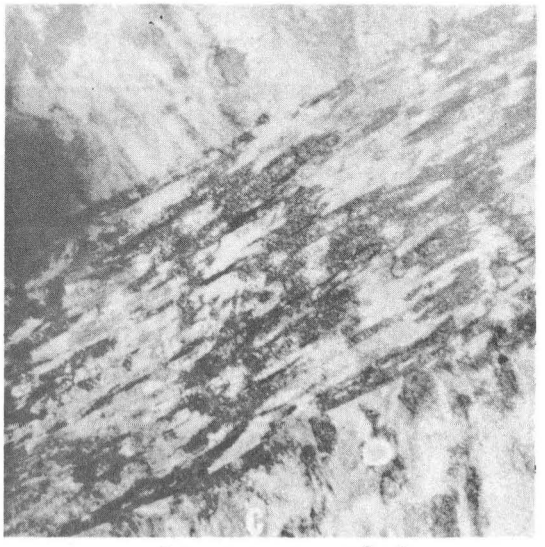

α [Tested at -196°C]

Fe, 9Cr, 8 Ni, 2Mn, 2Si, 1Mo, ·95V, ·08N, ·3C TRIP Steel

XBB708-3532

Fig. 11.

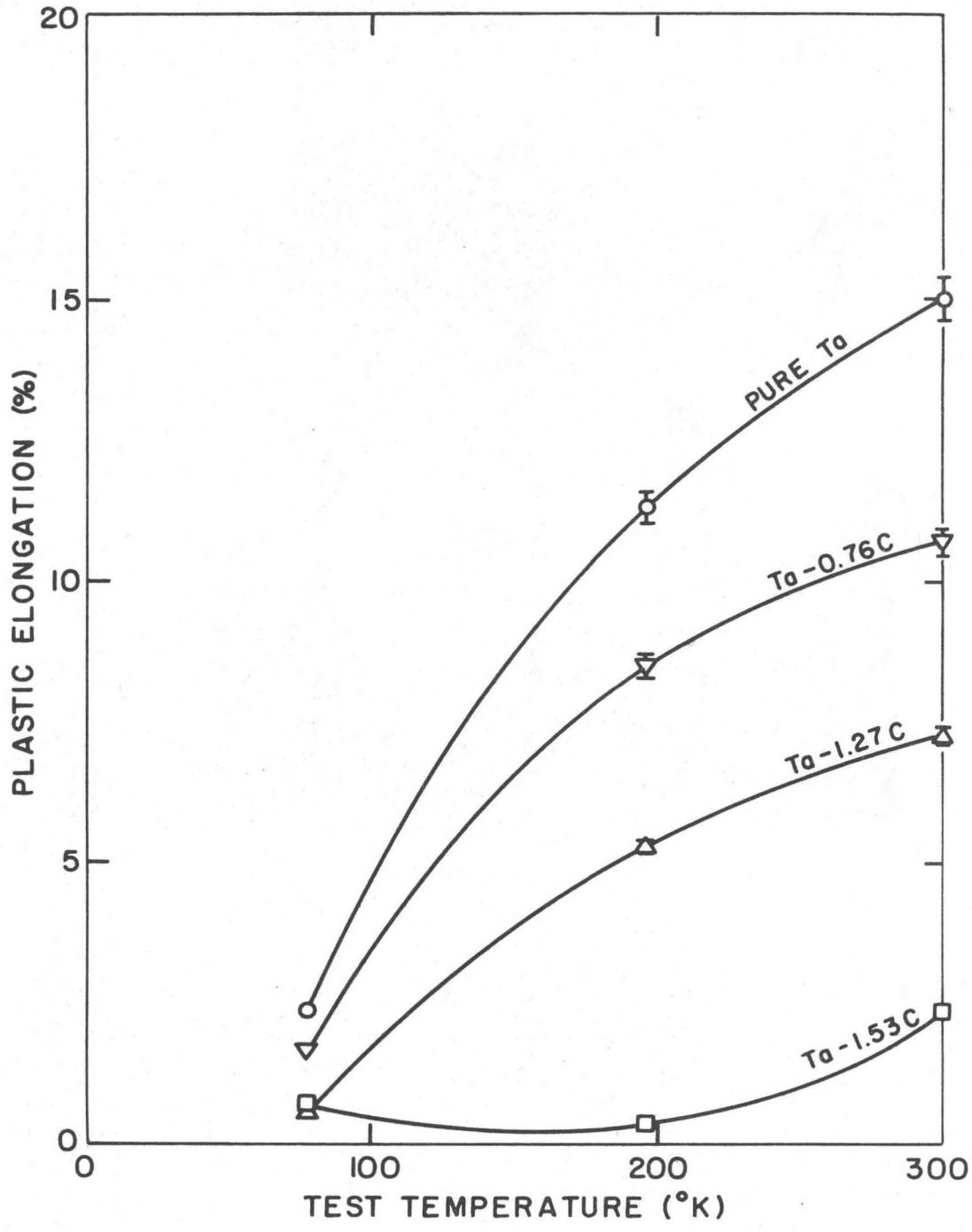
20
15
10
5
0
0
100
200
300
PLASTIC ELONGATION (%)
TEST TEMPERATURE (°K)
PURE Ta
Ta-0.76C
Ta-1.27C
Ta-1.53C
XBL 6910-5969

Fig. 12.

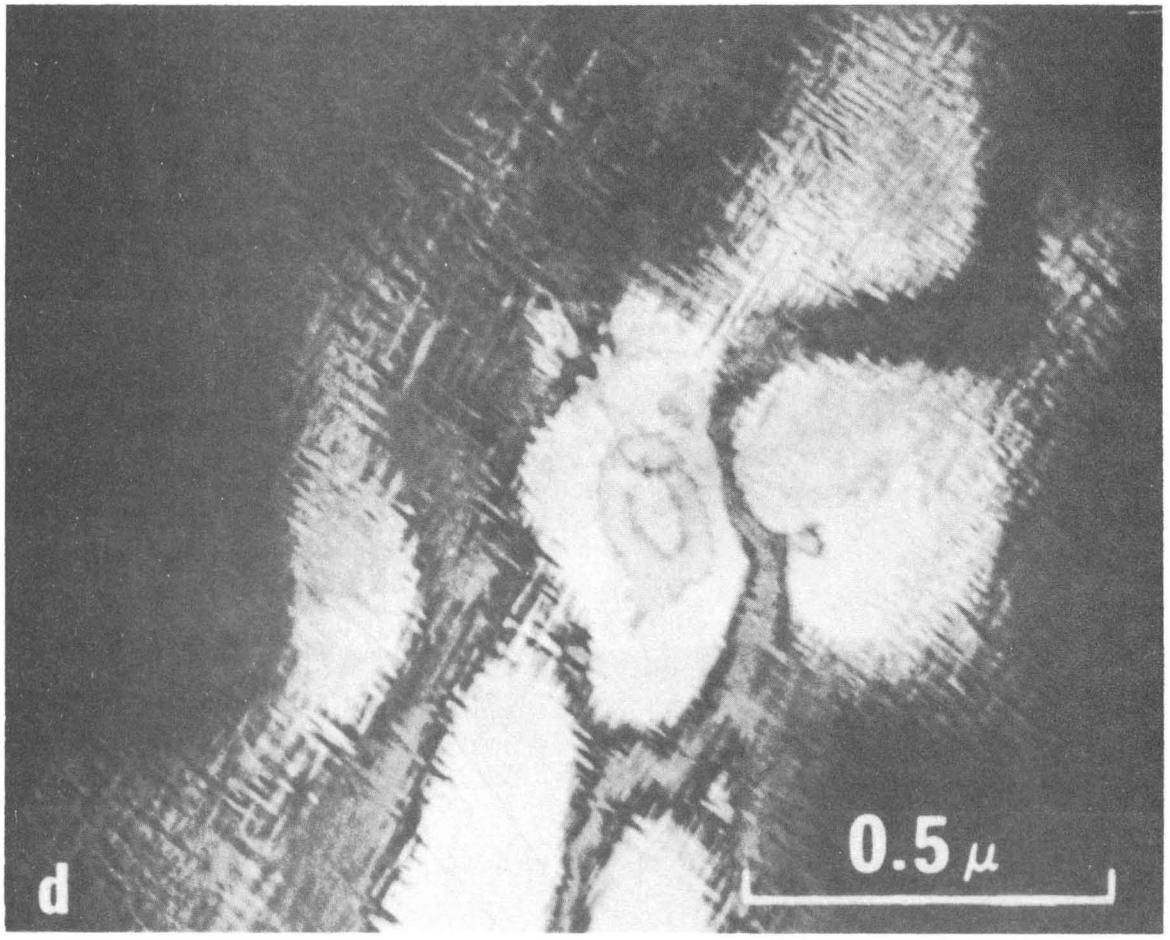

XBB6910-5969

Fig. 13.

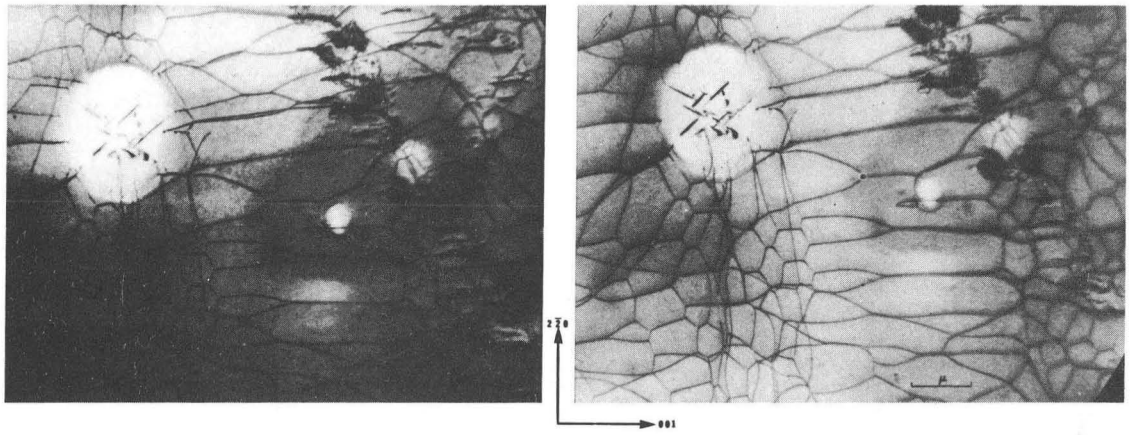

IM2295

Fig. 14.

IM2174

Fig. 15a.

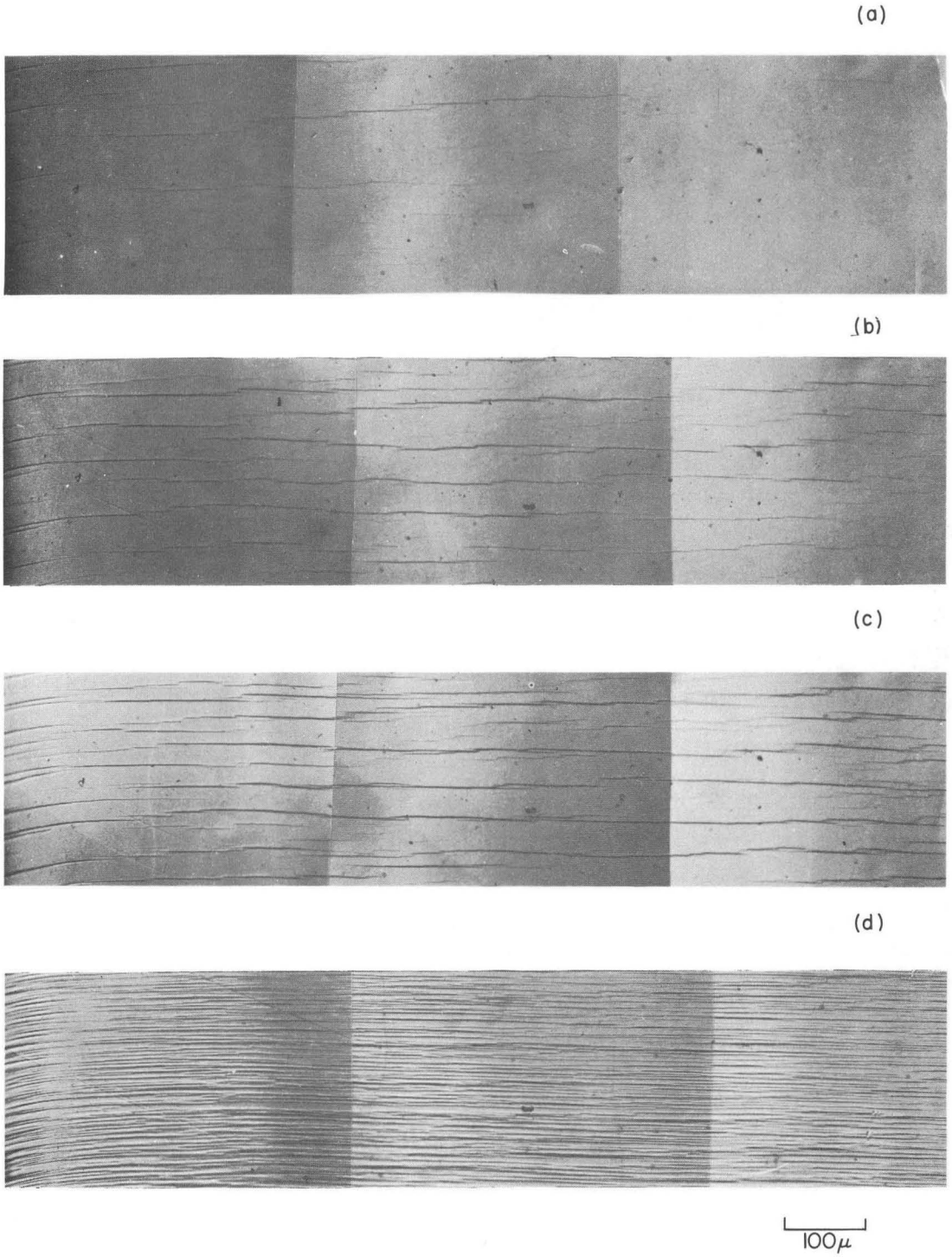

IM2180

Fig. 15b

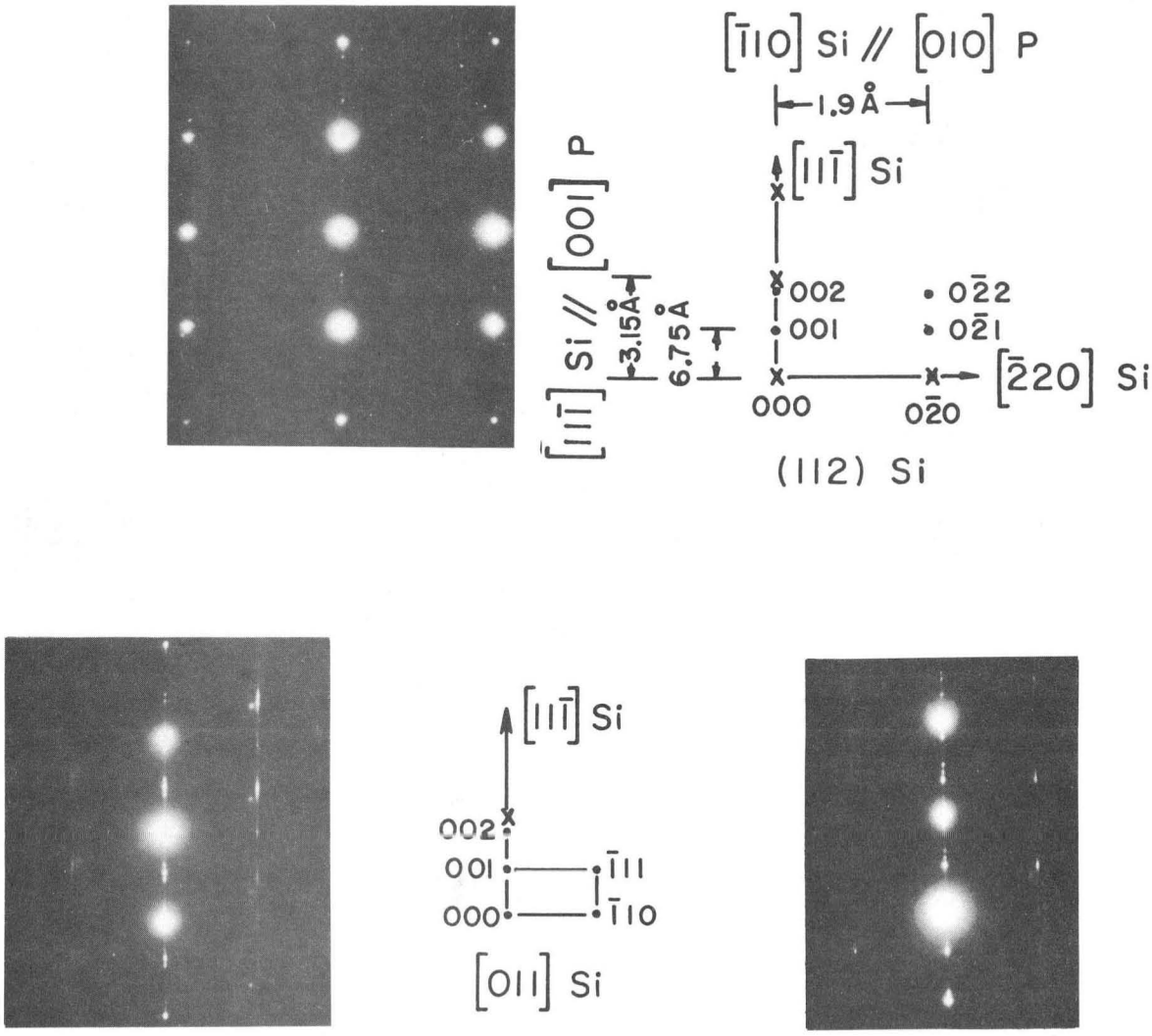
[1̄10] Si // [010] P
1.9Å
[111̄] Si
002
001
000
0̄22
0̄21
0̄20
[2̄20] Si
[001] P
Si //
3.15Å
6.75Å
[11̄1̄]
(112) Si
[111̄] Si
002
001
000
1̄11
1̄10
[011] Si
IM2168

Fig. 16.

TECHNICAL INFORMATION DIVISION
LAWRENCE RADIATION LABORATORY
UNIVERSITY OF CALIFORNIA
BERKELEY, CALIFORNIA 94720